Classical trajectory Monte Carlo calculation of the recoil-ion momentum distribution for positron-impact ionization collisions

2012 J. Phys. B: At. Mol. Opt. Phys. 45 065202

(http://iopscience.iop.org/0953-4075/45/6/065202)

J. Phys. B: At. Mol. Opt. Phys. **45** (2012) 065202 (9pp) doi:10.1088/0953-4075/45/6/065202

Classical trajectory Monte Carlo calculation of the recoil-ion momentum distribution for positron-impact ionization collisions

R O Barrachina and J Fiol

Centro Atómico Bariloche and Instituto Balseiro (Comisión Nacional de Energía Atómica and Universidad Nacional de Cuyo), 8400 S C de Bariloche, Río Negro, Argentina

E-mail: barra@cab.cnea.gov.ar and fiol@cab.cnea.gov.ar

Received 12 December 2011, in final form 30 January 2012
Published 29 February 2012
Online at stacks.iop.org/JPhysB/45/065202

Abstract
We investigate ionization processes induced by positron impact on H_2 by studying the momentum distributions of the receding ion. To this end, we employ classical trajectory Monte Carlo techniques. The investigation of the recoil ion momentum distribution allows us to shed new light on some known phenomena like the familiar 'electron capture to the continuum' peak of electron momentum spectroscopy, and also to unveil new structures which—up to our knowledge—have never been reported in the literature. We propose that some of these new effects represent fingerprints of a strong orientation of low-energy electrons into the direction of motion of the electron–positron centre of mass. We analyse the mechanisms that might give rise to these effects, and relate them to structures in the electron and positron momentum distributions. We also discuss how these theoretical predictions can be put to test in actual positron reaction microscopic experiments.

(Some figures may appear in colour only in the online journal)

1. Introduction

For several years, reaction microscopes have been used extensively and with great success to study inelastic collisions of photons and ions with atomic and molecular targets (e.g. [1, 2] and references therein). These novel techniques make it possible to measure the momenta of different fragments resulting from the collision, and even to determine fully differential cross sections to obtain kinematically complete pictures of the process. In this context, the ongoing experimental progress towards the use of reaction microscopes in conjunction with positron and positronium impact [3, 4] promises new research possibilities in a field where the extremely valuable study of differential cross sections (e.g. [5, 6] and references therein) has been mainly devoted to total and single differential cross sections and over very limited ranges.

The aim of this paper is to use classical trajectory Monte Carlo (CTMC) techniques in order to explore the possibility that the newly developed positron reaction microscopy would reveal some completely unforeseen structures of the positron-impact ionization cross section, or even similar or akin to those already observed with the traditional electron and momentum spectroscopy [7]. For instance, in 1998 the UCL group [8–10] measured positron-impact ionization processes in a forward collinear geometry (i.e. with the electron and the positron moving in the forward direction) and provided undubitable evidence of a peak in the electron energy distribution. This effect had been predicted by Brauner and Briggs [11] in 1986 as equivalent to the well-known 'electron capture to the continuum' (ECC) cusp of ion–impact collisions.

But when it comes to ionization or charge–exchange collisions, one of the distinguishing features of the reaction microscope is its ability to measure the energy and angular distribution of all or some of the outgoing particles, but mainly of the recoiling ion, simultaneously over the full 4π solid angle. This means that, instead of scanning the collision region by rotating the analyser as in any standard spectroscopy

technique, all the collision events can be detected at once, which greatly increases the accuracy and reduces measuring times. The distribution of the recoil-ion momentum (RIM) $\boldsymbol{K}_{\rm R}$ carries a great deal of information about the collision process, and represents an obvious choice to be the first to be explored with a positron reaction microscope [6]. Following this experimental lead, in this paper we investigate the ionization cross section $\mathrm{d}\sigma/\mathrm{d}\boldsymbol{K}_{\rm R}$ for positron impact, pinpointing its main structures and characteristics.

2. Theory and computational procedure

Let us study the ionization of hydrogen-like atoms of effective nuclear charge Z by the impact of energetic positrons. To this end we employ CTMC simulations [12, 13]. This method is well known and has been successfully applied to a variety of collision processes with electrons, positrons and ions in a great variety of situations, with incident velocities ranging from tenths to tens of atomic units [14, 15].

We numerically solve Hamilton's canonical equations for the three-body system for more than 10^8 trajectories by means of a modified middle-point code with adaptive step-size control [12, 13]. The initial conditions for each trajectory are characterized by six pseudo-random variables: the impact parameter of the incoming positron, three Euler angles fixing the plane and orientation of the target Kepler orbit in space, and the eccentricity and eccentric angle that define the shape of the target orbit and the initial position of the electron along this orbit, respectively [16]. The energy of the initial target orbit, whose centre of mass is initially at rest in the laboratory reference frame, is $\varepsilon_i = -Z^2 \times 13.6$ eV. In the laboratory reference frame, the velocity of the positron of energy E (given in eV) is $v = \sqrt{E/13.6}$ atomic units. From this point on, atomic units will be used throughout the paper except where explicitly indicated. The velocity of the centre of mass of the whole system reads $\boldsymbol{v}_{\rm CM} = \boldsymbol{v}/(M+2)$, where M is the mass of the target nucleus. The total energy in the centre-of-mass reference frame reads $E_{\rm CM} = \mu_T v^2/2 + \epsilon_i$, where $\mu_T = (M+1)/(M+2)$ is the reduced mass of the initial positron–target configuration [17].

The equations of motion are integrated until the momenta $\boldsymbol{k}_+$, $\boldsymbol{k}_-$ and $\boldsymbol{K}_{\rm R}$ of the positron, the electron and the nucleus in the laboratory reference frame converge, and the direct, ionization and positronium formation channels can be neatly separated according to energy criteria. It is noteworthy that low-energy ionization and high-excited capture events are difficult to separate. In the present work, trajectories evolution has been computed and monitored to long times until convergence was achieved with a relative error in energy of about 0.1%.

After convergence is achieved the differential cross section in a general set of variables $x_1, \ldots, x_N$ is evaluated by the formula

$$\frac{\mathrm{d}\sigma}{\mathrm{d}x_1, \ldots, \mathrm{d}x_N} = \frac{N_i(x_1, \ldots, x_N)/\Delta x_1, \ldots, \Delta x_N}{N/(\pi b_{\rm max}^2)},$$

where $N_i(x_1, \ldots, x_N)$ is the number of events of interest such that the variables $x_1, \ldots, x_N$ are in the neighborhood $\Delta x_1, \ldots, \Delta x_N$ of their given values. The events are normalized to the incident flux $N/\pi b_{\rm max}^2$, where N is the total number of trajectories and $b_{\rm max}$ is the maximum impact parameter evaluated. The standard deviation limit for these cross sections is given by [18]

$$\frac{\Delta\sigma}{\sigma} = \left[\frac{(N-N_i)}{NN_i}\right]^{1/2}.$$

For future convenience, we introduce the momentum

$$\boldsymbol{K} = M_{\rm R}\boldsymbol{v}_{\rm CM} - \boldsymbol{K}_{\rm R}, \tag{1}$$

which is related to the motion with respect to the residual target (of mass $M_{\rm R}$) of the centre of mass of all the other particles in the final state. For instance, for a direct process (elastic or excitation collisions), $M_{\rm R} = M+1$ and $\boldsymbol{K}$ is the momentum of the positron with respect to the target; while for positronium formation or single ionization, $\boldsymbol{K}$ is associated with the motion of the centre of mass of the electron–positron system (being it bound or in the continuum, respectively) with respect to the residual target ion of mass $M_{\rm R} = M$.

Within the ionization channel we also introduce the momenta $\boldsymbol{k}$ associated with the motion of the electron relative to the positron, so that

$$\boldsymbol{k}_\pm = \boldsymbol{v}_{\rm CM} \pm \boldsymbol{k} + \boldsymbol{K}/2\,. \tag{2}$$

The pair $(\boldsymbol{k}, \boldsymbol{K})$ is one of the three different sets of Jacobi momenta usually used to describe the kinematics of a three-body system in the centre-of-mass reference frame [19].

Let us note that the axial symmetry around the initial direction of motion of the positron reduces the number of relevant parameters of the cross section for the recoil-ion

$$\frac{\mathrm{d}\sigma}{\mathrm{d}\boldsymbol{K}} \equiv \frac{\mathrm{d}\sigma}{\mathrm{d}\boldsymbol{K}_{\rm R}} \tag{3}$$

to only two. For instance, let us consider the decomposition of the vectors $\boldsymbol{K}$ or $\boldsymbol{K}_{\rm R}$ into their components parallel ($K_{||}$, $K_{\rm R\,||}$) and perpendicular ($\boldsymbol{K}_\perp$, $\boldsymbol{K}_{\rm R\perp}$) to $\boldsymbol{v}_{\rm CM}$,

$$K_{||} = M_{\rm R}v_{\rm CM} - K_{\rm R\,||}, \qquad \boldsymbol{K}_\perp = -\boldsymbol{K}_{\rm R\perp}\,. \tag{4}$$

The parallel recoil momentum is a scalar magnitude while the perpendicular component is a two-dimensional vector in the plane perpendicular to $\boldsymbol{v}_{\rm CM}$. The recoil momentum distributions are independent of the choice of the plane in which the perpendicular component lies. Thus,

$$\frac{\mathrm{d}\sigma}{\mathrm{d}\boldsymbol{K}} = \frac{1}{2\pi K_\perp}\frac{\mathrm{d}\sigma}{\mathrm{d}K_\perp\,\mathrm{d}K_{||}} \equiv \frac{\mathrm{d}\sigma}{\mathrm{d}\boldsymbol{K}_{\rm R}} = \frac{1}{2\pi K_{\rm R\perp}}\frac{\mathrm{d}\sigma}{\mathrm{d}K_{\rm R\perp}\,\mathrm{d}K_{\rm R\,||}}. \tag{5}$$

In this case $K_\perp$ and $K_{\rm R\perp}$ refer to the magnitude of the vectors in the plane perpendicular to $\boldsymbol{v}_{\rm CM}$.

Another possible choice is to use the modulus and azimuthal angle with respect to $\boldsymbol{v}$ of either $\boldsymbol{K}$ or $\boldsymbol{K}_{\rm R}$. We define the angles θ and $\theta_{\rm R}$ such that $\cos\theta = \hat{\boldsymbol{K}}\cdot\hat{\boldsymbol{v}}$ and $\cos\theta_{\rm R} = \hat{\boldsymbol{K}}_{\rm R}\cdot\hat{\boldsymbol{v}}$, respectively:

$$\frac{\mathrm{d}\sigma}{\mathrm{d}\boldsymbol{K}} = \frac{1}{2\pi K^2\,\sin\theta}\frac{\mathrm{d}\sigma}{\mathrm{d}K\,\mathrm{d}\theta} \equiv \frac{\mathrm{d}\sigma}{\mathrm{d}\boldsymbol{K}_{\rm R}} = \frac{1}{2\pi K_{\rm R}^2\,\sin\theta_{\rm R}}\frac{\mathrm{d}\sigma}{\mathrm{d}K_{\rm R}\,\mathrm{d}\theta_{\rm R}}. \tag{6}$$

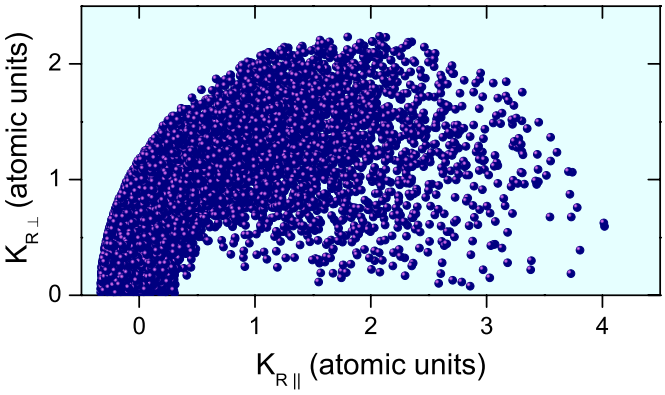

Figure 1. Distribution of the final (RIM) $\boldsymbol{K}_{\rm R}$ for 10^4 trajectories corresponding to the ionization of H_2 molecules by 50 eV positron impact. $K_{\rm R||}$ and $K_{\rm R\perp}$ are the components of $\boldsymbol{K}_{\rm R}$ parallel and perpendicular to the initial projectile velocity $\boldsymbol{v}$, respectively.

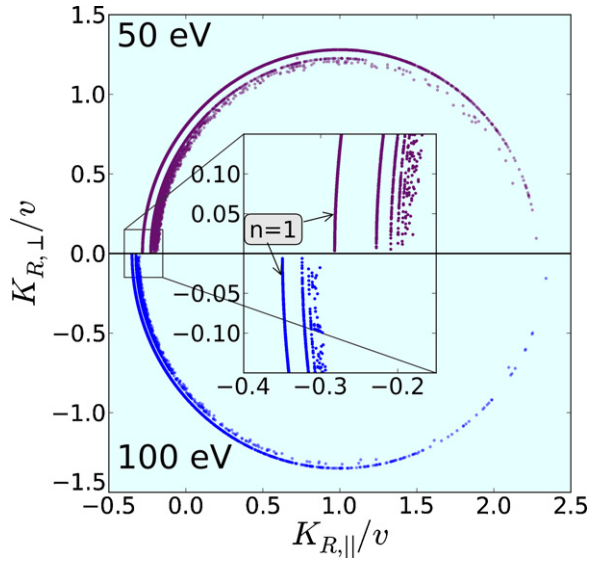

Figure 2. RIM distribution for positronium formation to bound states in 50 and 100 eV $e^+ + H_2$ collisions.

3. Ionization

Let us start our analysis by calculating a simple distribution of the final (RIM) $\boldsymbol{K}_{\rm R}$ for the single ionization of H_2 molecules by the impact of 50 eV positrons (initial velocity $v \approx 1.92$ au). Here, we model the molecule as a hydrogen-like atom with an effective charge Z given by the corresponding ionization energy, $\varepsilon_i = -15.603$ eV. A simple CTMC calculation performed over only 10^4 ionization trajectories is shown in figure 1.

Some characteristics of this figure immediately strike the eye.

- $\boldsymbol{K}_{\rm R}$ lies 'within' an 'outer' sphere centred at about the initial velocity of the positron.
- The edge of this 'outer' sphere is extremely sharp, i.e. the cross section $\mathrm{d}\sigma/\mathrm{d}\boldsymbol{K}_{\rm R}$ does not vanish at the border of this sphere, but seems to attain a finite value.
- The RIM distribution increases with increasing values of the azimuthal angle θ.
- There seems to be a sudden drop in the RIM distribution within a concentric 'inner' sphere.
- There is an almost absolute lack of ionization events when the RIM lies just below the inner sphere in the vicinity of the collision axis of symmetry.

In the following sections we analyse these effects in full detail.

4. Ionization threshold

The confinement of $\boldsymbol{K}_{\rm R}$ within a sphere in momentum space can be easily explained as a restriction imposed by energy conservation. In the centre-of-mass reference frame it reads

$$E_{\rm CM} = K^2/2\mu_P + k^2, \tag{7}$$

where $\mu_P = 2M/(M+2)$ is the reduced mass associated with the motion of the electron–positron pair with respect to the recoiling ion. This equation limits the range of values that $\boldsymbol{K}$ (or $\boldsymbol{K}_{\rm R}$) can attain. For instance, since in the ionization channel k is a real positive number, the associated Jacobi momenta $\boldsymbol{K}$ are confined within a sphere of radius $K_\circ = \sqrt{2\mu_P E_{\rm CM}}$, namely

$$K \leqslant K_\circ = \sqrt{2\mu_P E_{\rm CM}}, \tag{8}$$

as shown in figure 1. Note that while this condition is very simply written in terms of the magnitude of the Jacobi momentum $\boldsymbol{K}$, the equivalent expression in terms of the recoil momentum, i.e. $|\boldsymbol{K}_{\rm R} - \mu_P \boldsymbol{v}/2| \leqslant K_\circ$, involves both the magnitude $K_{\rm R}$ and angle $\theta_{\rm R}$ in a slightly more complex and cumbersome form,

$$K_{\rm R}^2 - K_{\rm R}\mu_P v\cos\theta_{\rm R} \leqslant \mu_P v^2/2 + 2\mu_P\varepsilon_i. \tag{9}$$

4.1. Positronium formation

Now, what lies beyond this outer sphere in momentum space? Resorting to (7) we see that for $K > K_\circ$ the electron–positron systems attain a negative energy, i.e. the positronium is formed [7]. To analyse this channel within the CTMC method, let us 'quantize' the positronium bound states by means of the procedure developed by Becker and MacKellar [20]. Whenever the energy

$$\epsilon = \left(K_\circ^2 - K^2\right)/2\mu_P \tag{10}$$

falls within the range

$$-\frac{1}{4}\left[n\left(n-\frac{1}{2}\right)(n-1)\right]^{-2/3} \leqslant \epsilon < -\frac{1}{4}\left[n\left(n+\frac{1}{2}\right)(n+1)\right]^{-2/3}, \tag{11}$$

for a given natural number n, we redefine the modulus of the momentum $\boldsymbol{K}$ as follows [12] :

$$K = \sqrt{K_\circ^2 + \mu_P/2n^2}. \tag{12}$$

We see in figure 2 that the RIM distribution for positronium concentrates on spheres that are concentric with and external to the outer sphere in figure 1. In particular, the sphere of largest

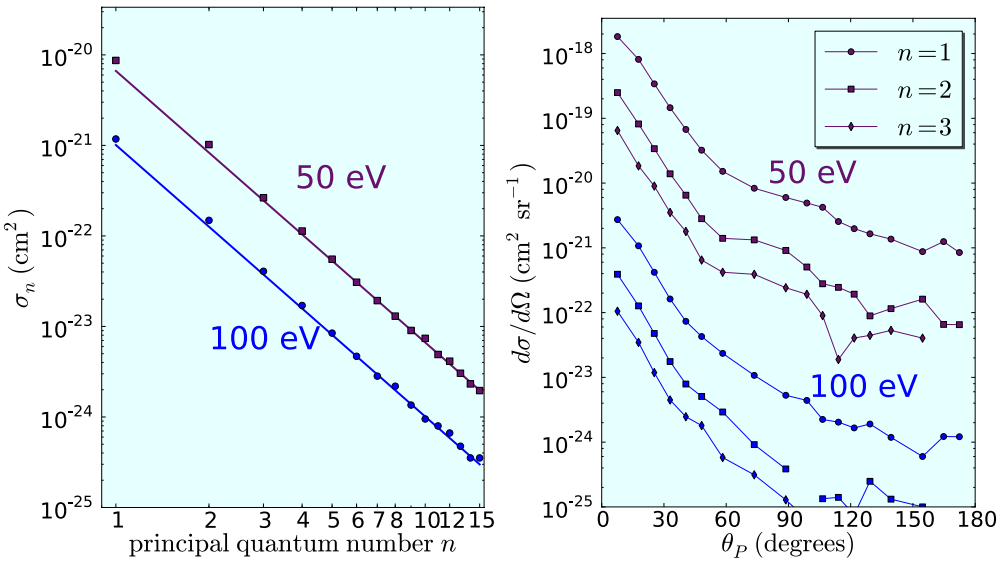

Figure 3. Calculated CTMC total and angular differential cross sections for positronium formation to bound states of principal quantum number n in 50 and 100 eV $e^+ + H_2$ collisions. More than 7 10^6 trajectories were evaluated. The differential cross sections for 50 eV have been multiplied by a factor of 100 to improve visualization.

possible radius, $K_{1s} = \sqrt{2\mu_P(E_{CM} + 1/4)}$, corresponds to the formation of ground-state positronium. The radius of the sphere systematically decreases as the electron is captured to higher excited states of the positronium, asymptotically approaching the threshold value $K_\circ$ as $n \to \infty$.

Figure 3 shows the total cross section and angular distributions for positronium formation in collisions of 50 and 100 eV positrons with H_2 as a function of the angle θ_P between the vector $\boldsymbol{K}$ and $\boldsymbol{v}$. At the investigated energies the electrons are predominantly captured to the ground state. The total charge-exchange cross sections to higher excited states follow the well-known Jackson–Schiff scaling rule $\sigma_n \propto n^{-3}$, characteristic of long-range final state interactions [21].

4.2. Longitudinal RIM distribution

The threshold shown in figure 1 was discovered 15 years ago by Rodríguez, Wang and Lin [22, 23]. Five years later, this finding was experimentally confirmed by Weber *et al* (2001) [24] for swift proton–helium collisions. They measured the ionization single differential cross section as a function of the parallel component $K_{R||}$ of the RIM, and found that it clearly attains a constant value at threshold. Unfortunately, a similar measurement in a positron-impact ionization collision would not produce a similar result, as it is shown in figure 4. This does not mean that the RIM distribution vanishes at the threshold. In contrast, we shall demonstrate that it attains a constant value as proposed in section 3, but that this threshold structure cannot be observed in the single differential cross section $d\sigma/dK_{R||}$. The reason for this discrepancy between ion- and positron-impact collisions is that, due to the different mass ratios, in the former case the limiting sphere can be approximated by a plane in the region where the RIM distribution is larger, and therefore the threshold structure can be observed directly in

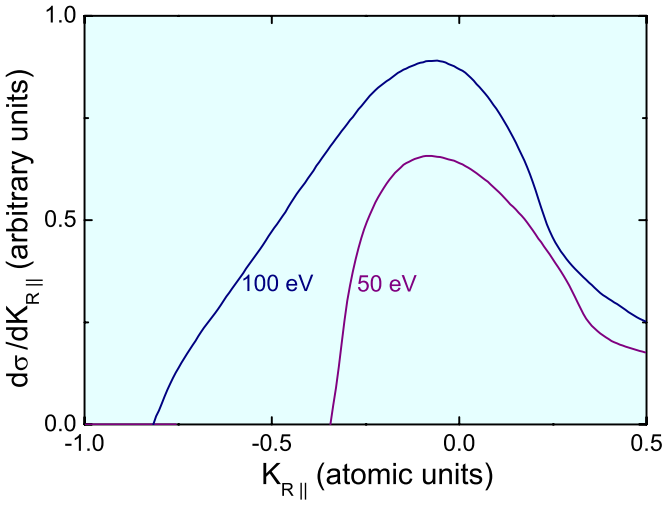

Figure 4. CTMC cross section for the ionization of H_2 molecules by 50 and 100 keV positron impact, single differential in the RIM component $\Delta K_{R||}$ parallel to the initial projectile velocity $\boldsymbol{v}$.

the single differential cross section $d\sigma/dK_{R||}$. This is no longer true for positron impact.

However, it should still be possible to observe the threshold structure in $K_{R||}$ by restricting the transversal component $K_{R\perp}$ to a narrow slit in momentum space. In figure 5, we see how the threshold structure builds up for diminishing acceptances $\Delta K_{R\perp}$. Unfortunately, this effect is accompanied by a progressive worsening of the statistics, that might even prevent the confirmation of this effect in future reaction microscopy experiments. As shown in figure 5 for the ionization of H_2 molecules by 100 eV positrons, when $\Delta K_{R\perp}$ is small enough for the threshold effect to be clearly observable, the statistics have worsened by more than one order of magnitude.

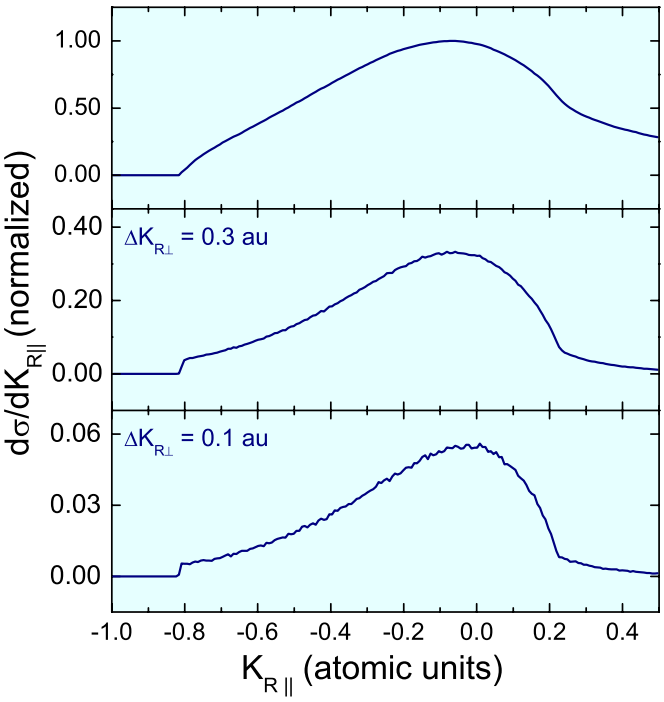

Figure 5. Cross section for the ionization of H_2 molecules by 100 keV positron impact, single differential in the RIM component $K_{R||}$ parallel to the initial projectile velocity $\boldsymbol{v}$ for different ranges in the perpendicular component. The cross section smoothly vanishes when no restriction is imposed as shown in the top panel, but the threshold becomes sharper for decreasing acceptance in $\Delta K_{R\perp}$. In the limit of perfect resolution the cross section will present a discontinuity at the threshold.

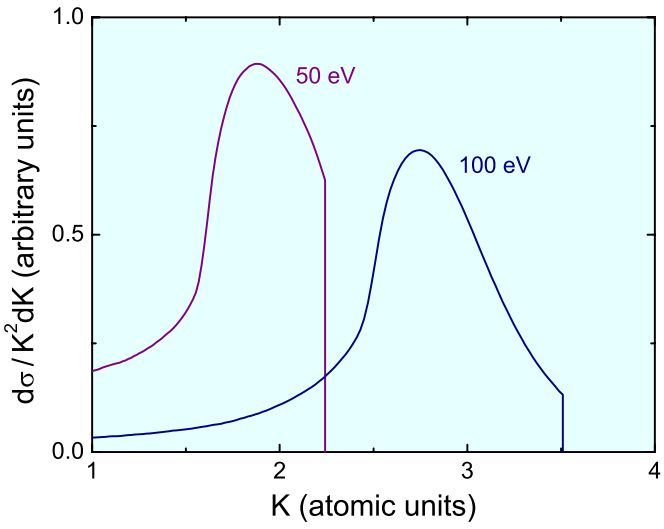

Figure 6. Cross section for the ionization of H_2 molecules by 50 and 100 keV positron impact, single differential in the modulus of the Jacobi momentum $\boldsymbol{K}$.

In spite of this shortcoming, we shall demonstrate that the aforementioned effect for positron-impact ionization collisions is likely to be observed in reaction microscope experiments, and with a significative resolution. The basic idea is to employ (1) to evaluate the single differential cross section in the modulus of the Jacobi momentum $\boldsymbol{K}$. In figure 6 we show the single differential cross section

$$\frac{\mathrm{d}\sigma}{K^2\,\mathrm{d}K} = \int \mathrm{d}\Omega_{\boldsymbol{K}}\,\frac{\mathrm{d}\sigma}{\mathrm{d}\boldsymbol{K}}, \tag{13}$$

for the single ionization of H_2 molecules by the impact of 50 and 100 keV positrons. We clearly see that the RIM distribution gets a constant value at this $K \to K_\circ$ threshold, and with no loss of statistics, since every ionization event is contributing to this cross section. It is obvious from the figure that the effect would be much more visible for smaller impact energies. Actually for 100 eV the ratio of the threshold with respect to the maximum of the RIM distribution is of the order of 20%, but it rises to 70% for an impact energy of 50 eV.

4.3. Final state interaction description

Where does this 'non-zero' value attained by the RIM distribution at threshold come from? The fact that, due to energy conservation, K reaches its limiting value $K_\circ$ when the electron–positron system is at the $k = 0$ threshold, obviously suggests that there has to be a relation between both limits. Actually, as was demonstrated by Rodríguez *et al* [22], the threshold in the momentum distribution of the recoiling target ion is directly related to the divergence of the ECC cusp structure at the origin of the distribution of the companion Jacobi momentum $\boldsymbol{k}$ for the electron–positron relative motion. This cusp-shaped peak was experimentally discovered 40 years ago by Crooks and Rudd [25] in energetic proton–hydrogen ionization collisions. Its presence in positron-impact collisions was demonstrated in 1998 by Kövér and Laricchia [8] in the ionization of H_2 molecules, and later corroborated by further experiments [9, 10], continuum distorted wave (CDW) calculations [19, 26] and CTMC simulations [13, 27]. In particular, CTMC is specially well suited for describing the ECC peak whenever certain precautions regarding convergence are taken [28].

On very general grounds, the fully differential cross section for the ionization by positron impact can be written as (see [7, 17, 21, 29–31] and references therein)

$$\frac{\mathrm{d}\sigma}{\mathrm{d}\boldsymbol{k}\,\mathrm{d}\Omega_{\boldsymbol{K}}} = F(k)\,\frac{\mathrm{d}\tilde{\sigma}}{\mathrm{d}\boldsymbol{k}\,\mathrm{d}\Omega_{\boldsymbol{K}}}, \tag{14}$$

where the distortion factor

$$F(k) = \frac{2\pi/k}{1-\exp(-2\pi/k)}, \tag{15}$$

diverges as $2\pi/k$ when $k \to 0$, while the reduced cross section $\mathrm{d}\tilde{\sigma}/\mathrm{d}\boldsymbol{k}\,\mathrm{d}\Omega_{\boldsymbol{K}}$ is a non-singular function of k at $k = 0$. This divergence is associated with the long-range nature of the electron-projectile Coulomb interaction in the final state [21]. Now, by using the energy conservation law (7) to change the momentum in (14) from $\boldsymbol{k}$ to $\boldsymbol{K}$ we obtain

$$\frac{\mathrm{d}\sigma}{\mathrm{d}\boldsymbol{K}} = \frac{kF(k)}{2\mu_P K}\int \frac{\mathrm{d}\tilde{\sigma}}{\mathrm{d}\boldsymbol{k}\,\mathrm{d}\Omega_{\boldsymbol{K}}}\,\mathrm{d}\Omega_{\boldsymbol{k}}, \tag{16}$$

with $k = \sqrt{(K_\circ^2 - K^2)/2\mu_P}$. Thus, this RIM cross section does not diverge or vanish for $K \approx K_\circ$, but defines a finite angle-dependent function

$$\lim_{K\to K_\circ}\frac{\mathrm{d}\sigma}{\mathrm{d}\boldsymbol{K}} = \frac{2\pi}{2\mu_P K_\circ}\,\mathcal{B}(\theta), \tag{17}$$

with

$$\mathcal{B}(\theta) = \int \left.\frac{\mathrm{d}\tilde{\sigma}}{\mathrm{d}\boldsymbol{k}\,\mathrm{d}\Omega_{\boldsymbol{K}}}\right|_{k=0} \mathrm{d}\Omega_{\boldsymbol{k}}, \tag{18}$$

as observed in figures 1, 5 and 6.

4.4. Continuation argument

We have demonstrated that the finite value achieved by the RIM cross section at the threshold between the ionization and the positronium formation channel is related to the appearance of the ECC peak in the electron–positron momentum distributions. Similarly, it can be easily demonstrated that it is also related by continuation arguments to a well-known scaling rule [32]. Actually, it can be shown that the cross section σ_n for the formation of highly excited bound states of principal quantum number n verifies

$$\sigma_n \propto 1/n^3\,. \tag{19}$$

This law, discovered by Oppenheimer in 1928 [33] and stated by Jackson and Schiff in 1953 [34] for charge-exchange processes in ion–atom collisions, can be generalized to the case of positron impact and, with a different dependence on n, to any set of bound states of arbitrary two-body potentials [21].

Now, in the positronium formation channel, the differential cross section as a function of the binding energy $\epsilon_n = -1/4n^2$,

$$\frac{\mathrm{d}\sigma}{\mathrm{d}\epsilon_n} = \frac{\sigma_n}{|\mathrm{d}\epsilon_n/\mathrm{d}n|} \approx 2n^3\sigma_n, \tag{20}$$

tends to a constant value for $n \to \infty$. Thus, by changing variables from ϵ_n to $K = \sqrt{K_\circ^2 - \epsilon_n}$ we find out that also the differential cross section as a function of the modulus of K does not diverge or vanish. Thus, we see that by simple continuation arguments, the 'non-zero' value of the RIM distribution at the threshold can be related to the presence of an accumulation point of positronium bound states at zero energy.

4.5. Dynamical entanglement

The previous result represents the simpler case of a fragmentation process, where one 'test' particle (i.e. the recoiling ion) balances the energy and momentum of a continuous N-body system (i.e. the electron–positron pair) on the verge of clustering. Actually, equation (14) is relating the RIM differential cross section $\mathrm{d}\sigma/\mathrm{d}\boldsymbol{K}_\mathrm{R} = \mathrm{d}\sigma/\mathrm{d}\boldsymbol{K}$ with the distortion factor $F(k)$, which is exclusively associated with the electron–positron continuous system thorough the $r \to 0$ limit of the radial s wavefunction, namely $|\psi_{0,k}(r)|^2 \underset{r\to 0}{\approx} F(k) \times (kr)^2$ [7]. Let us mention that this relation provides the main clue for studying other fragmentation processes with non-Coulombic two-body interaction [35, 36], as it might happen in positronium collisions [7].

Thus, equation (14) describes a *dynamical entanglement* of the test particle to the remaining system, as it was originally proposed by Watson in 1952 [37]. This means that the recoil-ion provides an indirect way of investigating the electron–positron system without even measuring any of these two particles. In particular, the $K \to K_\circ$ limit of the RIM distribution $\mathrm{d}\sigma/\mathrm{d}\boldsymbol{K}$ is sensing the behaviour of the electron–positron system in its very low-energy regime, i.e. $k \to 0$. The fact that $\mathrm{d}\sigma/\mathrm{d}\boldsymbol{K}$ goes to a constant value is related to the fact that the cross section differential in their kinetic energy k^2 also reaches a constant value according to Wigner's threshold law [38].

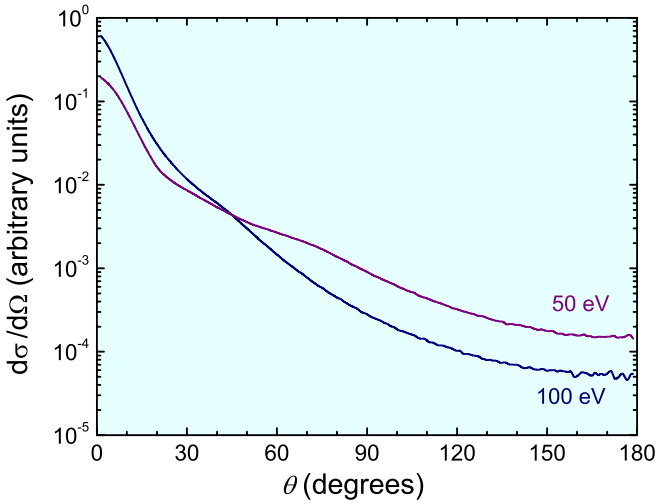

Figure 7. Cross section for the ionization of H_2 molecules by 50 and 100 keV positrons, differential in the orientation of the Jacobi momentum $\boldsymbol{K}$.

5. Angular distribution

In figure 7 we show the single differential cross section

$$\frac{\mathrm{d}\sigma}{\mathrm{d}\Omega_{\boldsymbol{K}}} = \int K^2\,\frac{\mathrm{d}\sigma}{\mathrm{d}\boldsymbol{K}}\,\mathrm{d}K, \tag{21}$$

as a function of the angle θ subtended by the Jacobi momentum $\boldsymbol{K}$ with respect to the initial direction $\hat{\boldsymbol{v}}$. In this figure it is evident that the RIM distribution is strongly oriented, with a drastic drop of more than three orders of magnitude between the forward and backward directions for 50 eV and four orders of magnitude for 100 eV. The width at half-maximum is of the order of only 8° and 6°, respectively. This very sharp angular dependence clearly indicates that the ionization occurs preferably with the electron–positron centre of mass moving in the forward direction in the final state, and the recoil-ion lagging behind it, as suggested by figure 1.

6. Second threshold

The RIM distribution in figure 1 shows that the ionization process is strongly suppressed within an inner sphere in the neighborhood of the symmetry axis. This effect is also quite evident in the contour plot of figure 8. The RIM distribution does not only drops sharply for values of K larger than $K_\circ = \sqrt{2\mu_P E_\mathrm{CM}}$ as described in section 3, but also within a concentric 'inner' sphere with a given radius K_in. For both cases of 50 and 100 eV, the radii of the inner and outer spheres seem to be in a ratio $K_\circ/K_\mathrm{in} \approx \sqrt{2}$. Resorting to the energy conservation equation (7), we find that this condition occurs whenever the velocity of the electron or the positron with

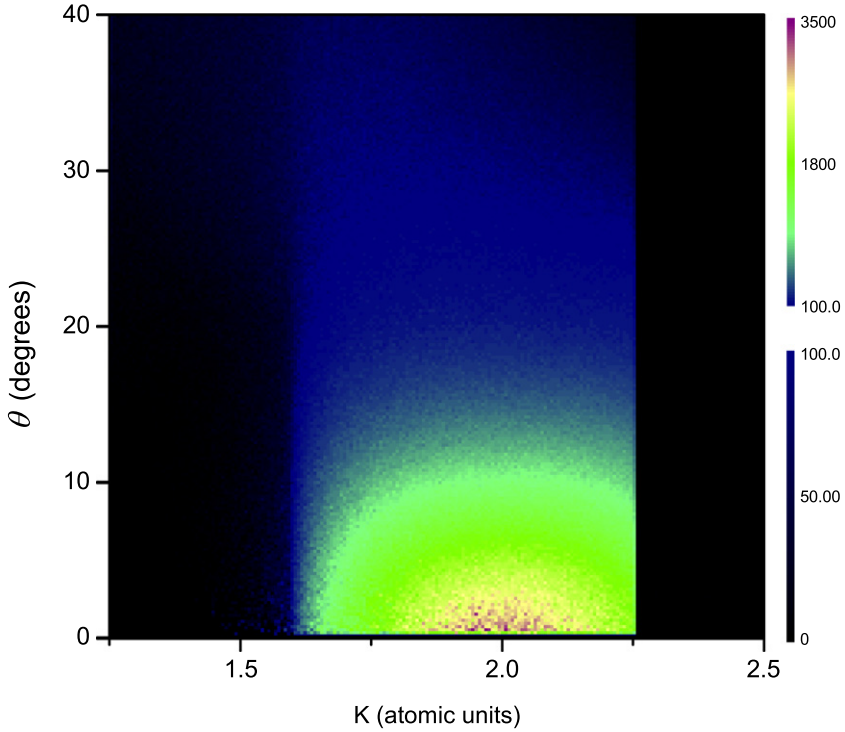

Figure 8. Contour plot of the cross section for the ionization of H_2 molecules by 50 eV positrons, doubly differential in the modulus K and azimuthal angle θ of the Jacobi momentum $\boldsymbol{K}$. Note that two different scales were used to highlight the threshold structure.

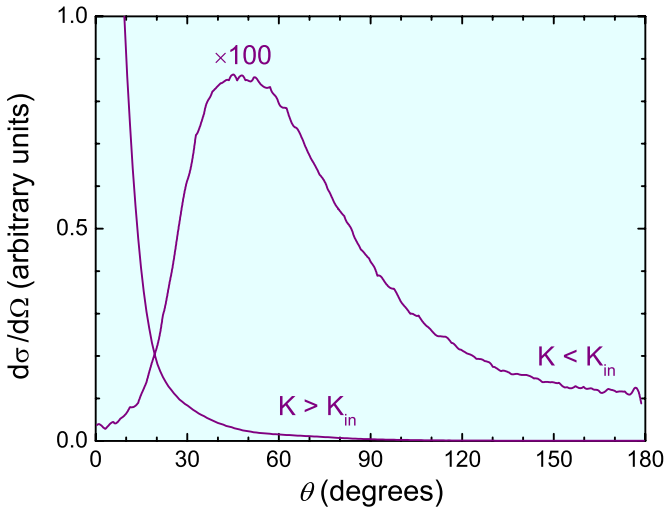

Figure 9. Cross section for the ionization of H_2 molecules by 50 eV positrons, single differential in the azimuthal angle θ of the Jacobi momentum $\boldsymbol{K}$. The curves correspond to values of the modulus K larger or smaller than $K_{\rm in}$.

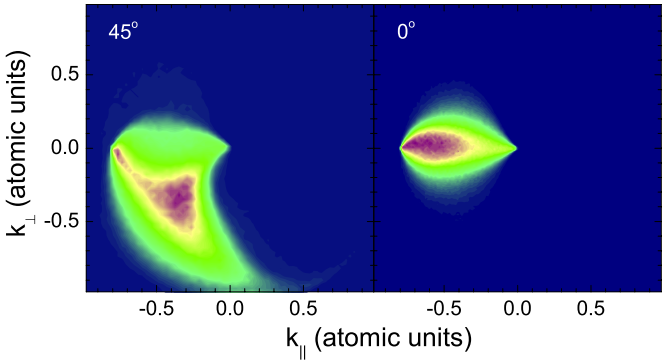

Figure 10. Projection of the cross section for the ionization of H_2 molecules by 50 keV positron impact in the plane formed by the Jacobi momentum $\boldsymbol{K}$ and the initial velocity $\boldsymbol{v}$. $k_{||}$ and $k_{\perp}$ are the components of the electron–positron relative momentum $\boldsymbol{k}$ parallel and perpendicular to the direction of motion of the corresponding centre of mass. The figures correspond to $\theta = 0^\circ$ and $\theta = 45^\circ$ as indicated, within an uncertainty of 5°.

respect to their centre of mass equals in modulus to that of this same centre of mass relative to the recoiling ion, namely $K/\mu_P = k$. Actually, this condition corresponds to a relation

$$\frac{K_\circ}{K_{\rm in}} = \sqrt{\frac{2(M+1)}{M}}, \tag{22}$$

between the radii of the outer and inner spheres. The situation is such that, whenever the Jacobi momentum K is in this range, the electron and positron velocities in a reference system attached to their centre of mass are smaller than that of the recoiling ion. Up to our knowledge, no similar result has ever been reported or investigated in ionization processes. We assume that this surprising effect might be related to a strong orientation of low-energy electrons into the direction of motion of the electron–positron centre of mass, already observed in our most recent CTMC calculations of the electron and positron momentum distributions [39, 40].

As it is shown in figure 1, there is a notorious depletion of the RIM distribution just below the inner sphere in the vicinity of the forward direction. This is clearly seen in figure 9, where the RIM distribution gets a minimum at $\theta = 0$, when

the modulus of the Jacobi impulse $\boldsymbol{K}$ is restricted to values inside the inner sphere, while it rises sharply when $K > K_{\rm in}$. This means that the inner sphere is more sharply defined when the electron–positron centre of mass moves in the forward direction. This result is consistent with CTMC calculations of the electron momentum distribution [30, 39, 40]. This means that the orientation effect of low-energy electrons described in the previous section is much stronger when θ is smaller. This can actually be observed in figure 10, where the distribution of the electron–positron relative momentum is more sharply focused for $\theta = 0^\circ$ than for $\theta = 45^\circ$.

7. Conclusions

In this paper, we have used the classical trajectory Monte Carlo (CTMC) model in order to find and describe the main characteristics of the recoil-ion momentum (RIM) distributions in positron-impact ionization processes. Some of them are similar to well-known effects observed in ion-impact ionization collisions. This is the case of the threshold between the ionization and positronium formation channels described in section 4. Others, mainly the possible existence of an inner sphere and the accompanying depletion of ionization events along the collision axis, as studied in section 6, have not been discussed previously in the literature. We have also analysed the mechanisms that might give rise to these different effects, and related them to structures in the electron and positron momentum distributions.

Naturally, these theoretical predictions should have to sustain the validation or refutation of RIM experiments, that might be put at reach imminently by positron reaction microscopic techniques. In particular, we have paid special attention to those structures that should be much easier to visualize in actual RIM experiments. In particular, we have shown how to define a single differential cross section that displays the threshold much more conspicuously than the actual distribution in the RIM. Certainly, this might represent a good first candidate to be measured in future positron reaction microscopic experiments.

Many if not all the effects described in this paper clearly show that the full three-body dynamics plays a dominant role in the description of positron-impact ionization processes. These are fully taken into account in CTMC calculations. On the other hand, high-order perturbative quantum theories like the CDW approximation have been very successful in describing most of the features of the electron and positron momentum distribution in ion [19, 41, 42] and positron [19, 26, 43, 44] impact ionization collisions. However, up to our knowledge, the strong orientation of the electron–positron dipole, which is responsible for the appearance of the inner sphere and the accompanying depletion at $\theta = 0$, is not described within any available quantum mechanical model [30, 31]. Much theoretical research along this line would be certainly needed in order to get a full and comprehensive picture of positron-impact reactions.

Acknowledgments

This work was partially supported by the Consejo Nacional de Investigaciones Científicas y Técnicas (grant PIP 112-200801-01269), Universidad Nacional de Cuyo (grant 06/C340) and Fundación Balseiro, Argentina. The authors are also members of the Consejo National de Investigaciones Científicas y Técnicas (CONICET), Argentina.

References

[1] Dörner R, Mergel V, Jagutzki O, Spielberger L, Ullrich J, Moshammer R and Schmidt-Böcking H 2000 *Phys. Rep.* **330** 95–192
[2] Ullrich J, Moshammer R, Dorn A, Dörner R, Schmidt L Ph H and Schmidt-Böcking H 2003 *Rep. Prog. Phys.* **66** 1463–545
[3] Slaughter D S, Hargreaves L R, Stevenson M A, Dorn A, Sullivan J P, Lower J C, Buckman S J and Lohmann B 2009 *J. Phys.: Conf. Ser.* **194** 2002
[4] Williams A I, Kövér Á, Murtagh D J and Laricchia G 2010 *J. Phys.: Conf. Ser.* **199** 2025
[5] Laricchia G, Armitage S, Köver Á and Murtagh D J 2009 *Advances in Atomic, Molecular and Optical Physics* vol 56 (Berlin: Academic) p 3
[6] Kövér Á, Murtagh D J, Williams A I and Laricchia G 2010 *J. Phys.: Conf. Ser.* **199** 12020
[7] Barrachina R O, Fiol J and Macri P 2008 *Nucl. Instrum. Methods* B **266** 402–6
[8] Kövér Á and Laricchia G 1998 *Phys. Rev. Lett.* **80** 5309–12
[9] Kövér Á, Paludan K and Laricchia G 2001 *J. Phys. B: At. Mol. Opt. Phys.* **34** L219–22
[10] Arcidiacono C, Kövér Á and Laricchia G 2005 *Phys. Rev. Lett.* **95** 223202
[11] Brauner M and Briggs J S 1986 *J. Phys. B: At. Mol. Opt. Phys.* **19** L325–30
[12] Fiol J, Courbin C, Rodríguez V D and Barrachina R O 2000 *J. Phys. B: At. Mol. Opt. Phys.* **33** 5343–55
[13] Fiol J and Olson R E 2002 *J. Phys. B: At. Mol. Opt. Phys.* **35** 1173–84
[14] Olson R E and Feeler C R 2001 *J. Phys. B: At. Mol. Opt. Phys.* **34** 1163–74
[15] Olson R E and Fiol J 2003 *J. Phys. B: At. Mol. Opt. Phys.* **36** L365–73
[16] Bandarage G and Parson R 1990 *Phys. Rev.* A **41** 5878–88
[17] Fiol J, Barrachina R O and Rodríguez V D 2002 *J. Phys. B: At. Mol. Opt. Phys.* **35** 149–64
[18] Schultz D R and Olson R E 1988 *Phys. Rev.* A **38** 1866–76
[19] Fiol J, Rodríguez V D and Barrachina R O 2001 *J. Phys. B: At. Mol. Opt. Phys.* **34** 933–44
[20] Becker R L and MacKellar A D 1984 *J. Phys. B: At. Mol. Opt. Phys.* **17** 3923–42
[21] Barrachina R O 1997 *Nucl. Instrum. Methods* B **124** 198–205
[22] Rodríguez V D, Wang Y D and Lin C D 1995 *Phys. Rev.* A **52** 9
[23] Rodríguez V D and Barrachina R O 1996 *Phys. Rev.* A **53** 3335–9
[24] Weber Th *et al* 2001 *Phys. Rev. Lett.* **86** 224–7
[25] Crooks G B and Rudd M E 1970 *Phys. Rev. Lett.* **25** 1599–601
[26] Berakdar J 1998 *Phys. Rev. Lett.* **81** 1393–6
[27] Tökési K 2007 *Radiat. Phys. Chem.* **76** 624–6
[28] Barrachina R O and Courbin C 2002 *J. Phys. B: At. Mol. Opt. Phys.* **35** 3157–65
[29] Barrachina R O and Sarkadi L 2005 *Nucl. Instrum. Methods* B **233** 260–5
[30] Fiol J and Barrachina R O 2009 *J. Phys. B: At. Mol. Opt. Phys.* **42** 231004

[31] Fiol J, Macri P and Barrachina R O 2009 *Nucl. Instrum. Methods* B **267** 211–4
[32] Barrachina R O 2005 *Nucl. Instrum. Methods* B **233** 19–27
[33] Oppenheimer J R 1928 *Phys. Rev.* **31** 349–356
[34] Jackson J D and Schiff H 1953 *Phys. Rev.* **89** 359–65
[35] Barrachina R O, Fiol J, Rodríguez V D and Macri P 2000 *The Physics of Electronic and Atomic Collisions* vol 500 (New York: AIP) pp 510–9
[36] Barrachina R O and Macri P A 2004 *Few-Body Syst.* **34** 175–80
[37] Watson K M 1952 *Phys. Rev.* **88** 1163–71
[38] Wigner E P 1948 *Phys. Rev.* **73** 1002–9
[39] Barrachina R O and Fiol J 2010 *J. Phys.: Conf. Ser.* **199** 12022
[40] Fiol J and Barrachina R O 2011 *J. Phys. B: At. Mol. Opt. Phys.* **44** 75205
[41] Fainstein P D, Ponce V H and Rivarola R D 1991 *J. Phys. B: At. Mol. Opt. Phys.* **24** 3091–119
[42] Crothers D S F and Dubé L J 1993 *Advances in Atomic, Molecular and Optical Physics* vol 30, ed D S F Crothers and L J Dubé (New York: Academic) p 287
[43] Della Picca R, Fiol J and Barrachina R O 2005 *Nucl. Instrum. Methods* B **233** 270–5
[44] Della Picca R, Fiol J, Barrachina R O and Rodríguez V D 2006 *Nucl. Instrum. Methods* B **247** 52–7